α-synuclein C-terminal Truncation Modulates Its Cytotoxicity and Aggregation by Promoting Its N-terminal Interactions With Membrane and Chaperone

Cai Zhang
Wuhan Institute of Physics and Mathematics, Innovation Academy for Precision Measurement Science and Technology, Chinese Academy of Sciences

Yunshan Pei
Wuhan Institute of Physics and Mathematics, Innovation Academy for Precision Measurement Science and Technology, Chinese Academy of Sciences

Zeting Zhang
Wuhan Institute of Physics and Mathematics, Innovation Academy for Precision Measurement Science and Technology, Chinese Academy of Sciences

Lingling Xu
Innovation Academy for Precision Measurement Science and Technology

Xiaoli Liu
Wuhan Institute of Physics and Mathematics, Innovation Academy for Precision Measurement Science and Technology, Chinese Academy of Sciences

Ling Jiang
Wuhan Institute of Physics and Mathematics, Innovation Academy for Precision Measurement Science and Technology, Chinese Academy of Sciences

Gary Pielak
University of North Carolina at Chapel Hill https://orcid.org/0000-0001-6307-542X

Xin Zhou
Wuhan Institute of Physics and Mathematics, Innovation Academy for Precision Measurement Science and Technology, Chinese Academy of Sciences

Maili Liu
Wuhan Institute of Physics and Mathematics, Innovation Academy for Precision Measurement Science and Technology, Chinese Academy of Sciences

Conggang Li (Conggangli@wipm.ac.cn)
Wuhan Institute of Physics and Mathematics, Innovation Academy for Precision Measurement Science and Technology, Chinese Academy of Sciences https://orcid.org/0000-0002-5798-1722

Article

Keywords: α-Synuclein, C-terminal truncation, membrane interactions, chaperones

Posted Date: January 24th, 2022

DOI: https://doi.org/10.21203/rs.3.rs-1151643/v1

Version of Record: A version of this preprint was published at Communications Biology on August 9th, 2022. See the published version at https://doi.org/10.1038/s42003-022-03768-0.

Abstract

α-synuclein (α-syn) is the main protein component of Lewy bodies, the major pathological hallmarks of Parkinson's disease (PD). C-terminal truncated forms of α-syn are found in the brain of PD patients, and reduce cell viability, as well as tend to form fibrils. Nevertheless, little is known about the molecular mechanisms underlying the role of C-terminal truncation on the cytotoxicity and aggregation of α-syn. The N-terminal domain of α-syn interacts with membranes and molecular chaperones, and these interactions are critical for the protein's physiological function and its pathological effects in PD. Here, we use nuclear magnetic resonance spectroscopy, a co-flotation assay, dynamic light scattering, and thioflavin T fluorescence to show that the truncation alters α-syn conformation, resulting in a new attractive interaction of the N-terminus with membranes and molecular chaperone, protein disulfide isomerase (PDI). Remarkably, the truncated protein is more toxic to mitochondria than full-length protein and diminishes the effect of PDI on α-syn fibrillation. Our findings reveal a modulatory role for the C-terminus in the cytotoxicity and aggregation of α-syn by interfering the interaction of the N-terminus with membrane and chaperone.

Significance Statement

α-synuclein is a Parkinson's Disease related protein, 15% of which is C-terminal truncated (CT-α-syn) in pathological inclusions. C-terminal truncation is shown to enhance the cytotoxicity and aggregation of α-syn, but the molecular mechanism behind these is not well understood. Here, we show that the more extended conformation of CT-α-syn favors the heterogeneous intermolecular interactions between α-syn with membrane and chaperone, which are critical for the physiological and pathological functions of α-syn. Remarkably, the enhanced interactions lead to mitochondrial dysfunction and disabled chaperone inhibition on fibrillation, highlighting the guard role of the C terminus on the cytotoxicity and aggregation of α-syn through intramolecular long-range interaction. This work provides a molecular basis for the pathological role of C-terminal truncation in PD.

Introduction

The soluble, disordered, monomeric protein, α-synuclein (α-syn) is abundant in presynaptic neurons and involved in neuronal function(1). Insoluble aggregates of α-syn in Lewy bodies (LBs) are the hallmark of Parkinson's disease (PD)(2, 3). α-syn's primary structure comprises three regions: the basic N-terminal domain (residues 1-60), which adopts an α-helix upon binding negatively charged membranes(4-6); the hydrophobic NAC domain (residues 61-95), which is prone to aggregation and form fibrils(7-9); and the flexible C-terminal domain (residues 96-140), which contains many negatively charged residues and interacts with cations and polyamines(10, 11).

Multiple forms of C-terminal truncated α-syn (CT-α-syn) are detected in normal and PD brains(12-16), and widely investigated due to their remarkable ability to aggregate and transform into pathologic fibrils. CT-α-syn accelerates formation of oligomers and fibrils compared to the full-length protein (FL-α-syn) *in*

vitro(17-27). When co-expressed with FL-α-syn, CT-α-syn promotes the pathological accumulation of FL-α-syn(28, 29). Deleting C-terminal residues accelerates aggregation up to residues 85-90, where the NAC domain begins. Further truncation decreases aggregation propensity because the NAC region forms the core of amyloid fibrils(7, 18, 30). Cells expressing CT-α-syn are more vulnerable to oxidative stress and CT-α-syn is more toxic than FL-α-syn(21, 31-33). Transgenic mice expressing C-terminal truncated species manifest PD-like symptoms(34). These observations suggest a role for CT-α-syn in PD, but the causes are unknown.

The compact conformation of monomeric α-syn is driven by long-range transient intramolecular interactions between the N- and C-termini(35, 36). In cells, the N-terminal domain interacts with membranes and chaperones that modulates fibrillation. For instance, the domain regulates fusion of synaptic vesicles and subsequent neurotransmitter release, which are critical for normal brain function(37, 38). Molecular chaperones, such as protein disulfide isomerase (PDI) and Hsp70, bind the N-terminal domain, dissolve and degrade accumulated misfolded α-syn, highlighting the role of chaperones in preventing α-syn aggregation and regulating its physiological function(39-41). These observations raise the question of whether C-terminal truncations affect the interaction of the N-terminal domain with membranes and chaperones, which could affect its functionality.

Here, we investigate the effects of C-terminal truncation. Nuclear magnetic resonance spectroscopy (NMR) and co-flotation data reveal a stronger interaction of N-terminus with membranes and with PDI, a major endoplasmic reticulum (ER) chaperone(42). The interaction may arise from the more extend conformation of CT-α-syn. The functional assay reveals severe mitochondrial membrane disruption by CT-α-syn compared to FL-α-syn in both neuronal cells and isolated mitochondria. Dramatically differential inhibitory effects of PDI on FL-α-syn and CT-α-syn fibrillation are also observed. Our results suggest that the C-terminus behaves like a ‘guard’ regulating α-syn function. The absence of this guard results in stronger membrane interaction, accelerated fibrillation and diminished chaperone inhibition, all of which could affect the etiology of PD.

Results

C-terminal truncation causes stronger interactions with membranes and PDI. α-syn forms an N-terminal α-helix upon binding negatively charged membranes, without involvement of the C-terminus(4), but it is not known if deleting the C-terminus affects binding. We prepared lipid mixtures comprising 1-palmitoyl-2-oleoyl-sn-glycero-3-phosphocholine (POPC)/1-palmitoly-2-oleoyl-sn-glycero-3-phosphate (POPA) (1:1 in mole ratio) to obtain highly anionic liposomes. Binding of FL- and CT-α-syn was analyzed by co-flotation, a common method for studying protein-membrane interaction. The principle is that bound and unbound proteins migrate differentially in iohexol gradients. Liposomes, and membrane associated proteins migrate to the top of the gradient and unbound proteins to the bottom (Figure 1B). The fractions from top to bottom were collected and quantified by sodium dodecyl sulfate polyacrylamide gel electrophoresis (SDS-PAGE) (Figure 1C and S1A). Approximately 80% of the CT-α-syn binds the membrane whereas ~50% of FL-α-syn is bound state (Figure 1D), indicating stronger association of CT-α-syn.

α-syn associates with mitochondrial membranes, whose major component is the anionic phospholipid cardiolipin (CL)(43). We acquired ^{1}H-^{15}N heteronuclear single quantum coherence (HSQC) spectra of uniformly ^{15}N-enriched FL- and CT-α-syn in the presence of liposomes comprising POPC/CL (9:1 and 7:3 mole ratio, respectively). NMR provides binding information at the residue level because resonances from strongly bound residues show reduced intensities(44). Analysis of spectra acquired in the absence and presence of liposomes (Figure 1E and S1B) indicate that, consistent with previous results, the N-terminus dominates binding(5). Data for CT-α-syn show that signals are more attenuated in the presence of liposomes containing CL, indicating a stronger binding of CT-α-syn to acidic lipids than FL-α-syn, consistent with co-flotation data.

Molecular chaperones are another important binding partner of the N-terminal region(45). PDI interacts with the hydrophobic region of the N-terminal region, inhibiting aggregation(41, 46). To investigate the impact of the C-terminal truncation on the interaction with PDI, we acquired ^{1}H-^{15}N HSQC spectra of uniformly ^{15}N-enriched FL- and CT-α-syn in the presence of PDI at a mole ratio of 2:1, which enabled us to assess intermolecular interactions at the residue level via chemical shift perturbations (CSPs) and intensity changes. PDI binds the first 10 residues of FL-α-syn (segment 1) and 10 residues near Tyr39 (segment 2) (Figure 2A and B). Both sites are located at the N-terminus, consistent with other reports(41, 45). Although the attenuation patterns of CT- and FL-α-syn in PDI are similar, there are changes in chemical shift and intensity (Fig 2C), suggesting the constructs have similar PDI-binding sites but different affinities. We quantified the dissociation constants (K_D) of FL- and CT-α-syn by fitting CSPs values as a function of PDI concentration (Figure 2D). Two segments of FL-α-syn show similar mM K_D values, whereas segment 1 of CT-α-syn has a K_D of ~39.3 μM, about an order magnitude increase in affinity of CT-α-syn for PDI.

C-terminal truncated α-syn exhibits a more extended conformation. Given the difference in membrane binding between FL- and CT-α-syn, we examined the constructs using PRE to determine whether deleting the C-terminus alters the ensemble of conformations. We prepared spin-labeled proteins by incorporating 1-oxyl-2,2,5,5-tetramethyl-delta3-pyrroline-3-methyl (MTSL), a paramagnetic spin label, into single cysteine variants (A90C) of ^{15}N-enriched FL- and CT-α-syn. Cross peaks arising from residues close to the label broaden due to enhanced transverse relaxation. As reported(35), intramolecular interactions between the N- and C-terminal regions lead to broadening proximal to the spin label and in residues within the N-terminal region, neighboring Tyr39 (Figure 3A). Similar intramolecular long-range interactions are absent in CT-α-syn. Its N-terminal residues show weak PRE, suggesting a more extended conformation for CT-α-syn (Figure 3B). We conclude that interactions between the N- and C-terminal regions cause the PRE effects observed in FL-α-syn.

Effects of C-terminus truncation on physiological and pathological functions. To better understand the membrane-related physiological differences between FL- and CT-α-syn, we evaluated the mitochondrial potential ($\Delta\Psi_m$) in living SK-N-SH cells using the dye, 5, 5', 6, 6'-tetrachloro-1, 1', 3, 3'-tetraethylbenzimidazolocarbocyanine iodide (JC-1). In normal cells, JC-1 aggregates in the matrix due to

the electrochemical potential gradient resulting in the red fluorescence. Apoptotic events cause monomeric JC-1 to disperse throughout the cell resulting in green fluorescence. Images were acquired after treatment with 50 μM FL- or CT-α-syn for 5 h. Mitochondria in untreated SK-N-SH cells stained bright red. Red fluorescence decreased markedly in CT-α-syn-incubated cells concomitant with an increase in green fluorescence, indicating collapse of the mitochondrial membrane potential (Figure 4A). The green/red fluorescence intensity ratio showed no significant difference between FL-α-syn-treated and control cells (Figure 4B). Thus, the C-terminal truncation increases mitochondrial damage compared to the negative control and FL-α-syn.

Next, we isolated mitochondria from SK-N-SH cells. Given the dissipated membrane potential, we anticipated mitochondrial membrane permeabilization, allowing cytochrome *c* (cyto *c*) release(47, 48). We assessed release after treatment with various concentrations of FL- and CT-α-syn after 1 h at 37 °C (Figure 4C) via Western blotting (WB). Enhanced release relative to control mitochondria was detected with CT-α-syn. We did not observe significant release of cyto *c* compared to controls with FL-α-syn. This result lends support to the idea that CT-α-syn disrupts mitochondrial membrane, leading to cyto c release.

To understand the influence of C-terminal truncation on membrane interactions, we used DLS to monitor formation of POPC/CL liposome clusters in the presence of FL- and CT-α-syn. FL-α-syn barely clusters liposomes while CT-α-syn dramatically increases particle size (Figure 4D and S3). The results agree with our NMR data showing that CT-α-syn interacts more strongly with liposomes than FL-α-syn. Hence, the ability of CT-α-syn to cluster liposomes suggests a stronger membrane interaction, which could disrupt membranes.

To shed light on chaperone binding and CT-α-syn aggregation, we used Thioflavin T (ThT) fluorescence to monitor the rate of CT-α-syn aggregation in the absence or presence of an equal molar ratio of PDI and compared the rate to that of FL-α-syn. The ß-sheet structure of amyloid fibrils binds ThT dye enhancing fluorescence(49). Figure 4E shows a typical nucleation-aggregation profile, beginning with a lag phase, followed by an elongation phase, and ending in a plateau. In the absence of PDI, truncation of the C-terminus accelerates CT-α-syn aggregation with a decreased lag time compared to FL-α-syn (Figure 4E, Table 1). This result points to an auto-inhibitory role for the C-terminus. As expected, the presence of PDI inhibits FL-α-syn aggregation(46, 50, 51), but inhibits CT-α-syn aggregation to a somewhat smaller extent, as reflected by an over 3-fold increase in lag time for FL-α-syn whereas less than 2-fold for CT-α-syn. Besides, half-time of aggregation ($t_{1/2}$) clearly show that PDI exerted a less inhibitory effect on CT-α-syn aggregation (Figure 4F), though the seg-1 of CT-α-syn interacts more strongly with PDI.

Discussion

Misfolded, oligomeric and fibrillar α-syn contribute to neuronal toxicity and progression of PD(52-54). The proposed transient long-range interaction between the N-terminus and acidic tail of α-syn may inhibit fibril formation(55). Releasing these contacts destabilizes the natively unfolded monomers potentiating aggregation(35, 56). For instance, Ca^{2+}, Cu^{2+} and polyamine binding alters α-syn's long-range interaction

exposing the amyloidogenic NAC region, resulting in enhanced fibrillation(57). We observe a similar conformational change for CT-α-syn. The results suggest that deleting the C-terminus disrupts the intramolecular long-range interaction between the N- and C-terminus such that CT-α-syn adopts a relatively extended conformation in which the N-terminus is more exposed (Figure 3B), resulting in faster aggregation of CT-α-syn compared to the full length protein. Moreover, the exposed N-terminus of monomeric CT-α-syn has a greater chance of recruiting fibrils(58). Consistent with previous reports, the C-terminus plays an auto-chaperoning role by shielding the amyloidogenic NAC region(20, 59-61).

Our finding that truncating the C-terminal region facilitates membrane binding contradicts a report purporting to show that the deletion has no effect(62). However, our NMR data (Figure 1E) show attenuated signals of CT-α-syn in the presence of liposomes compared to FL-α-syn, supporting our co-flotation data (Figure 1C-D) indicating more membrane bound CT-α-syn. The DLS data (Figure 4D) also demonstrate a stronger interaction of CT-α-syn with membrane. α-syn binds negatively charged membranes via electrostatic interactions between the membrane surface and the positively charged N-terminus(63). Hence, exposing the N-terminus increases anionic membrane binding.

Membrane interaction is a common cause of membrane disruption by the intrinsically disordered proteins(64). After establishing the stronger interaction of CT-α-syn with artificial mitochondrial membranes, we turned to the physiological effect on mitochondrial membrane potential in living SK-N-SH cells. Using JC-1 staining, the data (Figure 4A-B) show CT-α-syn collapses the potential, which coincides with cyto *c* release (Figure 4C). By contrast, FL-α-syn does not impact cyto *c* release or membrane potential. α-syn causes mitochondrial fragmentation, via direct interaction with mitochondrial membranes(65, 66). These fragmented mitochondria are present in neurons along with α-syn deposits(67). The stronger interaction of CT-α-syn with mitochondrial membranes may explain its disruptive ability.

Molecular chaperones help dissolve α-syn aggregates and prevent formation of pathological fibrils. For instance, Hsp70, a mammalian chaperone, breaks α-syn fibrils into monomers or oligomers(39, 40). The common chaperone binding region of α-syn is in the N-terminus. Our data showing that PDI binds two segments in the N-terminus (Figure 2A-C) are consistent with the result of Yagi-Utsumi et al(41). In addition, we find that segment 1 in CT-α-syn binds more tightly to PDI, while segment 2 has a similar binding affinity (Figure 2D). The stronger interaction of segment 1 diminishes the inhibitory effect of PDI on CT-α-syn aggregation (Figure 4E-F). Segment 2, comprising residues 36-42, is the master controller of α-syn aggregation at neutral pH(68). We hypothesize that the stronger interaction of PDI with segment 1 in CT-α-syn is the reason for the diminished inhibitory effect on aggregation. To test this idea, we changed Tyr39 to Glu (Y39E) in segment 2 to weaken its affinity for PDI. The mutation abolishes the interaction of segment 2 with PDI whereas segment 1 still bound tightly (Figure S4A-C). While $t_{1/2}$ of the variant in the absence of PDI was too long to measure, the ThT fluorescence assay indicates an increased aggregation rate in the presence of PDI, with $t_{1/2}$ of about 45 h (Table, Figure S4D-E). This observation suggests that segment 2 is a controller and segment 1 acts as accelerator of fibrillation. Our results reinforce the importance of residues near Tyr39 in manipulating aggregation, reveal the differential effect of segment

1 and 2 on the fibrillation upon binding PDI, and may provide a clue for chaperone-based design of fibrillation inhibitors.

Our results along with those others demonstrate that the C-terminus maintains α-syn's normal physiological function. It appears that the C-terminal region evolved to balance the interactions of the N-terminus with the membranes; strong interactions disrupt membranes causing toxicity, while weak interactions hobble neurotransmitter release. Chaperones help cells handle misfolded proteins, but when the C-terminus is truncated, α-syn fibrillation spins out of control. We propose a mechanism for how CT-α-syn might promote PD (Figure 5). Long-range interaction between the N- and C-terminal regions keep α-syn in its normal physiology-relevant conformation. Uncontrolled fibrillation occurs upon C-terminal truncation. Moreover, the stronger interaction between the CT-α-syn and mitochondrial membrane induces collapse of the mitochondrial membrane potential causing membrane permeability, cyto *c* release and buildup of mitochondrial reactive oxygen species (mtROS), activating the apoptosome and NLRP3 inflammasome(69-74). The activation of the inflammasome causes more truncation of FL-α-syn *in vivo* resulting in a negative-feedback loop, amplifying truncation, which elicits neuronal cell death and PD(75-77). Our observations show the importance of maintaining intact α-syn in cells. We propose that reducing C-terminal truncation is a plausible way to prevent the onset or development of PD.

Conclusion

Truncating the C-terminus releases long-range interaction between domains. CT-α-syn exhibits a more extended conformation, resulting in stronger interactions with membranes and molecular chaperones. The truncation also causes mitochondrial damage and accelerates fibrillation, both are key aspects of pathogenesis. The differential inhibitory fibrillation effects of PDI on FL- and CT-α-syn reveal opposite roles for the two segments in fibrillation. The C-terminus regulates, either directly, via metal ion- and polyamine-binding, or indirectly by modulating membrane and chaperone interactions. Once truncated, its control over the N-terminus is released, triggering mitochondrial damage and pathological fibrillation. In summary, the C-terminal domain is a 'guard'. In other words, the C-terminal domain plays an auto-inhibitory role in FL-α-syn by shielding the N-terminus, weakening interactions with membranes and chaperones. Our work also suggests that preventing truncation is a strategy for preventing the onset or development of PD and synucleinopathies(26, 27, 33, 78).

Materials And Methods

Protein expression and purification. α-syn mutants containing a deletion of the C-terminus (amino acids 1-99), single cysteine mutants and single glutamic acid mutant were generated by using site-directed mutagenesis. Natural abundance and ^{15}N-enriched α-syn and its variants were expressed in *Escherichia coli* BL21 (DE3) cells in either LB media or M9 minimal medium supplemented with $^{15}NH_4Cl$. The cells were grown at 37 °C to an optical density at 600 nm (OD_{600}) of 0.6 and induced with 1 mM isopropyl β-D-1- thiogalactopyranoside (IPTG) for 4 h. Cells were harvested by centrifugation at 6,300*g* for 10 min at 4

°C. FL-α-syn and FL-A90C were purified as described(79). For CT-α-syn and CT-A90C, cells were resuspended in 1 mM phenylmethanesulfonyl fluoride (PMSF), 50 mM MES, pH 6.0 and lysed in a high-pressure homogenizer (ATS Engineering). Cell lysates centrifuged at 48000*g* for 30 min at 4 °C. The supernatant was introduced into a SP cation exchange column (GE Healthcare) and the column eluted in a gradient of 0-1000 mM NaCl. Fractions containing the proteins were concentrated after SDS-PAGE analysis and then chromatographed on a Superdex 75 26/600 column (GE Healthcare) eluted with 50 mM MES and 200 mM NaCl, pH 6.0.

The human PDI gene was cloned into a pET-28a vector containing a His6-tag and a TEV protease cleavage site at the N terminus. The recombinant vector was transformed into *E. coli* BL21 (DE3). The cells were cultured in LB medium at 37 °C. When cell density reached an OD_{600} of 0.8, PDI expression was induced with 1 mM IPTG for 7 h. Cells harvested by centrifugation were resuspended in 20 mM Tris, 500 mM NaCl, pH 8.0 with freshly prepared 10mg/L protease inhibitors (Sigma-Aldrich). After lysis and centrifugation, the soluble fraction applied to a HisTrap column (GE Healthcare), which was eluted with a linear gradient of 0-500 mM imidazole. Protein was further purified by anion exchange chromatography with a Resource Q column (GE Healthcare) using 20 mM Tris, pH 8.0 and eluted by a linear gradient of 0-1000 mM NaCl, followed by size-exclusion chromatography with a Superdex 200 16/600 column (GE Healthcare) equilibrated with 20 mM Tris, 300 mM NaCl, pH 8.0. Protein concentration was determined either by absorbance of aromatic amino acids at 280 nm with a NanoDrop spectrophotometer (extinction coefficients is 5.96 and 1.49 for FL- and CT-α-syn, respectively), or by Bradford assay using BSA as a standard. Purified proteins were desalted using a HiTrap column (GE Healthcare), lyophilized and stored at -80 °C.

Liposome preparation. POPC, POPA and CL were purchased from Avanti Polar Lipids (Alabaster, AL) and used without purification. Liposomes containing 50% POPC and 50% POPA, and liposomes containing POPC and CL (mole ration of 9:1 for C1 liposomes and 7:3 for C3 liposomes) were prepared as described(79, 80).

Liposome co-flotation assay. Liposomes were incubated with FL- or CT-α-syn for 30 min at room temperature. An equal volume of iohexol [80% (w/v)] was added. The sample in 40% (w/v) iohexol was transferred to a thick-wall centrifugation tube (Beckman) before 300 µl of liposome buffer, 375 µl of 30% (w/v) iohexol and 375 µl of 35% (w/v) iohexol were added in that order without mixing. A SW60Ti rotor (Beckman) was used for gradient centrifugation at 28000*g* for 150 min at 4 °C. Lipid bound proteins were recovered from the 0% and 40% iohexol. The mixture was then deconstructed from the top into nine equal fractions prior to SDS-PAGE analysis. Image J software (National Institutes of Health) was used to quantify band intensity.

^{1}H-^{15}N Heteronuclear single quantum coherence (HSQC). Spectra from membrane-binding experiments were acquired using 0.1 mM ^{15}N-enriched FL- and CT-α-syn dissolved in NMR buffer (20 mM HEPES, 100 mM KCl, pH7.0) plus 10% (v/v) D_2O in the absence or presence of 12 mM liposomes. ^{1}H-^{15}N HSQC spectra from PDI binding experiments were acquired using 0.3 mM ^{15}N-enriched FL- and CT-α-syn

dissolved in 20 mM HEPES, 100 mM NaCl, 5 mM tris (2-carboxyethyl) phosphine (TCEP), pH 7.0, 10% (v/v) D_2O in the absence, or presence of PDI at mole ratios from 10:1 to 1:1. Experiments were carried out at 15 °C on a Bruker Avance 800 or 850 MHz NMR spectrometer. Resonance assignments for α-syn are available from the BioMagResBank (entry number 16543). Data were analyzed with Sparky software. Intensity ratios were calculated by peak heights in the presence and absence of liposomes or PDI. CSPs of backbone amides were calculated according to Eq. 1(81), where $\Delta\delta_H$ and $\Delta\delta_N$ denote the chemical shift difference in the absence and presence of PDI in the ^1H and ^{15}N dimension, respectively.

$$\Delta\delta = \sqrt{(\Delta\delta_H)^2 + 0.04 \cdot (\Delta\delta_N)^2} \quad 1$$

K_D was calculated using the fitting function shown in Eq. 2(82):

$$\Delta\delta_{obs} = \frac{^{\Delta\delta}_{\max}\left\{([P]_t+[L]_t+K_d)-\left[([P]_t+[L]_t+K_d)^2-4[P]_t[L]_t\right]^{1/2}\right\}}{2[P]_t} \quad 2$$

Where $\Delta\delta_{obs}$ is the observed FL- or CT-α-syn chemical shift minus the free FL- or CT-α-syn shifts, $[P]_t$ represents the concentration of FL- or CT-α-syn (300 mM), and $[L]_t$ represents PDI concentration, from 0 to 300 mM.

Paramagnetic relaxation enhancement (PRE). For spin label (MTSL) conjugation, single cysteine variants of ^{15}N-enriched FL- and CT-α-syn (FL- and CT-A90C) were dissolved in NMR buffer and reduced with 5 mM DTT for 30 min. The proteins were then reacted with a 5-fold mole excess of MTSL at 4 °C for 16 h in the dark. Excess MTSL was removed by eluting samples over a HiTrap desalting column (GE Healthcare) into NMR buffer. Complete labeling was confirmed by LC-MS. Spin-labeled FL- and CT-α-syn were lyophilized or used directly. Intramolecular PRE experiments required 100 μM ^{15}N-MTSL-labeled protein. PRE experiments were conducted in NMR buffer containing 10% (v/v) D_2O at 15 °C using a Bruker Avance 850-MHz spectrometer. Diamagnetic samples were prepared by adding a 10-fold mole excess of ascorbic acid to the paramagnetic samples. PRE data were processed using NMRpipe-software and analyzed with Sparky- software. PRE effects were quantified as the ratios of peak intensities recorded in the paramagnetic state versus the diamagnetic state, respectively. The transverse relaxation rate enhancements (R_2) were calculated with Eq. 3(83):

$$R_2 = \frac{1}{T_b - T_a} \ln \frac{I_{dia}(T_b) I_{para}(T_a)}{I_{dia}(T_a) I_{para}(T_b)} \quad 3$$

Where I_{dia}, I_{para} denote NMR signal intensity in the diamagnetic and paramagnetic state, respectively, the interval time T_b–T_a, was 17.2 ms for FL-α-syn and 20 ms for CT-α-syn.

Dynamic light scattering (DLS). FL- or CT-α-syn (20 μM) were incubated with 100 μM liposomes in a total volume of 1 ml of NMR buffer at room temperature for 30 min. Clustering activity was measured by DLS

using a Protein Solutions DynaPro instrument (Malvern) in triplicate, with an average of 10 data points. Particle size distribution of liposomes for control experiments was monitored under same conditions.

Cyto *c* release. At least 10^7 SK-N-SH cells were used per experiment. The mitochondria were prepared with a Mitochondria Isolation Kit (Solarbio) for cultured cells. The procedure is described previously(84). Briefly, freshly isolated mitochondria were resuspended in ice cold buffer (10 mM HEPES, 2 mM K_2HPO_4, 10 mM succinate, 250 mM sucrose, 1 mM ATP, 0.08 mM ADP, 1 mM DTT). Aliquots were incubated with FL- and CT-α-syn at 37 °C for 1h. After incubation, the mixture was centrifuged at 13000*g* at 4 °C for 10 min and the supernatant interrogated using SDS-PAGE followed by WB with an anti-cyto *c* monoclonal antibody (Abcam).

Mitochondrial membrane potential. SK-N-SH cells were incubated with 50 μM FL- and CT-α-syn 37 °C for 5 h. The JC-1 kit (Sigma-Aldrich) was used according to manual. Images were acquired with a confocal fluorescence microscope (Leica TCS SP8). Fluorescence intensity was analyzed with Image J software.

Fibrillation monitored by thioflavin T (ThT) fluorescence. Lyophilized FL- and CT-α-syn were dissolved in 20 mM Tris, 100 mM NaCl, 2 mM TCEP, pH 7.5, 0.01% (w/v) NaN_3 and filtered through a 0.22 μm Millex filter. A 1.5 mM ThT stock was prepared in same buffer. Samples (200 μl) containing either FL-/CT-α-syn or mixed with equivalent amount of PDI were dispensed along with a 2.5-mm glass bead in each well of a black, transparent bottomed, 96-well plate. The plate was sealed with a Al sealing tape (Corning) and incubated in a SpectroMax i3x microplate reader (Molecular Devices) at 37 °C with 500 s high-grade orbital shaking. ThT fluorescence was measured every 10 min using excitation and emission wavelengths of 444 nm and 482 nm, respectively. The data were analyzed using Eq. 4(11).

$$F(t) = F_0 + A/(1 + e^{-k(t-t_{1/2})}) \quad (4)$$

F(t) was normalized by dividing the largest value in each experiment, *k* represents the fibrillation rate constant and $t_{1/2}$ is the aggregation half-time. The lag time t_{lag} was calculated as: $t_{lag} = (t_{1/2} - 2/k)$.

Abbreviations

α-syn, α-synuclein; CL, cardiolipin; CSP, chemical shift perturbation; CT-α-syn, C-terminal truncated α-syn; cyto *c*, cytochrome *c*; DLS, dynamic light scattering; ER, endoplasmic reticulum; FL-α-syn, full-length α-syn; HSQC, heteronuclear single quantum coherence; IPTG, isopropyl β-D-1- thiogalactopyranoside; JC-1, 5, 5', 6, 6'-tetrachloro-1, 1', 3, 3'-tetraethylbenzimidazolocarbocyanine iodide; K_D, dissociation constant; LBs, Lewy bodies; mtROS, mitochondrial reactive oxygen species; MTSL, 1-oxyl-2,2,5,5-tetramethyl-Delta3-pyrroline-3-methyl; NMR, nuclear magnetic resonance; PD, Parkinson's disease; PDI, protein disulfide isomerase; PMSF, phenylmethanesulfonyl fluoride; POPA, 1-palmitoly-2-oleoyl-sn-glycero-3-phosphate; POPC, 1-palmitoyl-2-oleoyl-sn-glycero-3-phosphocholine; PRE, paramagnetic relaxation enhancement; SDS-PAGE, sodium dodecyl sulfate polyacrylamide gel electrophoresis; TCEP, tris (2-carboxyethyl) phosphine; ThT, thioflavin T; WB, Western blotting; $\Delta\Psi_m$, mitochondrial membrane potential.

Declarations

Acknowledgments

This work is supported by the Ministry of Science and Technology of China, the National Natural Sciences Foundation of China (21673284, 21925406 and 21991080), the National Key R&D Program of China (2018YFE0202302) and K. C. Wong Education Foundation.

Author Contributions

[#] These authors contribute equally to this work. Conceived and designed the experiments: CZ, YP, ZZ, LJ, GJP, XZ, ML, CL. Performed experiments: CZ, YP, ZZ, LX, XL. Analyzed data: CZ, YP, ZZ, LJ, GJP, XZ, ML, CL. Wrote paper: CZ, LJ, ZZ, GJP, XZ, ML, CL.

Competing Interest Statement

The authors declare no competing financial interests.

References

1. Benskey MJ, Perez RG, & Manfredsson FP. The contribution of alpha synuclein to neuronal survival and function - implications for Parkinson's disease. J. Neurochem. 137, 331-359 (2016).
2. Spillantini MG, et al. Alpha-synuclein in Lewy bodies. Nature 388, 839-840 (1997).
3. Spillantini MG, Crowther RA, Jakes R, Hasegawa M, & Goedert M. Alpha-synuclein in filamentous inclusions of Lewy bodies from Parkinson's disease and dementia with Lewy bodies. Proc. Natl. Acad. Sci. U. S. A. 95, 6469-6473 (1998).
4. Davidson WS, Jonas A, Clayton DF, & George JM. Stabilization of alpha-synuclein secondary structure upon binding to synthetic membranes. J. Biol. Chem. 273, 9443-9449 (1998).
5. Bartels T, et al. The N-terminus of the intrinsically disordered protein α-synuclein triggers membrane binding and helix folding. Biophys. J. 99, 2116-2124 (2010).
6. Eliezer D, Kutluay E, Bussell R, Jr., & Browne G. Conformational properties of alpha-synuclein in its free and lipid-associated states. J. Mol. Biol. 307, 1061-1073 (2001).
7. Giasson BI, Murray IV, Trojanowski JQ, & Lee VM. A hydrophobic stretch of 12 amino acid residues in the middle of alpha-synuclein is essential for filament assembly. J. Biol. Chem. 276, 2380-2386 (2001).
8. Rodriguez JA, et al. Structure of the toxic core of α-synuclein from invisible crystals. Nature 525, 486-490 (2015).
9. Cho MK, et al. Structural characterization of alpha-synuclein in an aggregation prone state. Protein Sci. 18, 1840-1846 (2009).

10. Fernandez CO, et al. NMR of alpha-synuclein-polyamine complexes elucidates the mechanism and kinetics of induced aggregation. EMBO J. 23, 2039-2046 (2004).
11. Eliezer D. The mysterious C-terminal tail of alpha-synuclein: Nanobody's guess. J. Mol. Biol. 425, 2393-2396 (2013).
12. Muntane G, Ferrer I, & Martinez-Vicente M. α-synuclein phosphorylation and truncation are normal events in the adult human brain. Neuroscience 200, 106-119 (2012).
13. Bhattacharjee P, et al. Mass spectrometric analysis of Lewy body-enriched α-synuclein in Parkinson's disease J. Proteome Res. 18, 2109-2120 (2019).
14. Delcourt V, et al. Spatially-resolved top-down proteomics bridged to MALDI MS imaging reveals the molecular physiome of brain regions. Mol. Cell. Proteomics 17, 357-372 (2018).
15. Anderson JP, et al. Phosphorylation of Ser-129 is the dominant pathological modification of alpha-synuclein in familial and sporadic Lewy body disease. J. Biol. Chem. 281, 29739-29752 (2006).
16. Li W, et al. Aggregation promoting C-terminal truncation of alpha-synuclein is a normal cellular process and is enhanced by the familial Parkinson's disease-linked mutations. Proc. Natl. Acad. Sci. U. S. A. 102, 2162-2167 (2005).
17. Sorrentino ZA, et al. Physiological C-terminal truncation of α-synuclein potentiates the prion-like formation of pathological inclusions. J. Biol. Chem. 293, 18914-18932 (2018).
18. Murray IV, et al. Role of alpha-synuclein carboxy-terminus on fibril formation in vitro. Biochemistry 42, 8530-8540 (2003).
19. Iyer A, et al. C-terminal truncated α-synuclein fibrils contain strongly twisted β-sheets. J. Am. Chem. Soc. 139, 15392-15400 (2017).
20. Levitan K, et al. Conserved C-terminal charge exerts a profound influence on the aggregation rate of α-synuclein. J. Mol. Biol. 411, 329-333 (2011).
21. Ma L, et al. C-terminal truncation exacerbates the aggregation and cytotoxicity of α-synuclein: A vicious cycle in Parkinson's disease. Biochim. Biophys. Acta, Mol. Basis Dis. 1864, 3714-3725 (2018).
22. Ni X, McGlinchey RP, Jiang J, & Lee JC. Structural insights into α-synuclein fibril polymorphism: effects of Parkinson's disease-related C-terminal truncations. J. Mol. Biol. 431, 3913-3919 (2019).
23. Van der Wateren IM, Knowles TPJ, Buell AK, Dobson CM, & Galvagnion C. C-terminal truncation of α-synuclein promotes amyloid fibril amplification at physiological pH. Chem. Sci. 9, 5506-5516 (2018).
24. Sorrentino ZA, Xia Y, Gorion KM, Hass E, & Giasson BI. Carboxy-terminal truncations of mouse α-synuclein alter aggregation and prion-like seeding. FEBS Lett. 594, 1271-1283 (2020).
25. McGlinchey RP, et al. C-terminal α-synuclein truncations are linked to cysteine cathepsin activity in Parkinson's disease. J. Biol. Chem. 294, 9973-9984 (2019).
26. Terada M, et al. The effect of truncation on prion-like properties of α-synuclein. J. Biol. Chem. 293, 13910-13920 (2018).
27. Games D, et al. Reducing C-terminal-truncated alpha-synuclein by immunotherapy attenuates neurodegeneration and propagation in Parkinson's disease-like models. J. Neurosci. 34, 9441-9454

(2014).
28. Ulusoy A, Febbraro F, Jensen PH, Kirik D, & Romero-Ramos M. Co-expression of C-terminal truncated alpha-synuclein enhances full-length alpha-synuclein-induced pathology. Eur. J. Neurosci. 32, 409-422 (2010).
29. Volpicelli-Daley LA, et al. Exogenous α-synuclein fibrils induce Lewy body pathology leading to synaptic dysfunction and neuron death. Neuron 72, 57-71 (2011).
30. Stephens AD, et al. Extent of N-terminus exposure of monomeric alpha-synuclein determines its aggregation propensity. Nat. Commun. 11, 2820 (2020).
31. Stefanova N, Klimaschewski L, Poewe W, Wenning GK, & Reindl M. Glial cell death induced by overexpression of alpha-synuclein. J. Neurosci. Res. 65, 432-438 (2001).
32. Kanda S, Bishop JF, Eglitis MA, Yang Y, & Mouradian MM. Enhanced vulnerability to oxidative stress by alpha-synuclein mutations and C-terminal truncation. Neuroscience 97, 279-284 (2000).
33. Bassil F, et al. Reducing C-terminal truncation mitigates synucleinopathy and neurodegeneration in a transgenic model of multiple system atrophy. Proc. Natl. Acad. Sci. U. S. A. 113, 9593-9598 (2016).
34. Daher JP, et al. Conditional transgenic mice expressing C-terminally truncated human alpha-synuclein (alphaSyn119) exhibit reduced striatal dopamine without loss of nigrostriatal pathway dopaminergic neurons. Mol. Neurodegener. 4, 34 (2009).
35. Bertoncini CW, et al. Release of long-range tertiary interactions potentiates aggregation of natively unstructured alpha-synuclein. Proc. Natl. Acad. Sci. U. S. A. 102, 1430-1435 (2005).
36. Dedmon MM, Lindorff-Larsen K, Christodoulou J, Vendruscolo M, & Dobson CM. Mapping long-range interactions in alpha-synuclein using spin-label NMR and ensemble molecular dynamics simulations. J. Am. Chem. Soc. 127, 476-477 (2005).
37. Zhang MY & Beyer CE. Measurement of neurotransmitters from extracellular fluid in brain by in vivo microdialysis and chromatography-mass spectrometry. J. Pharm. Biomed. Anal. 40, 492-499 (2006).
38. Watson JB, et al. Alterations in corticostriatal synaptic plasticity in mice overexpressing human alpha-synuclein. Neuroscience 159, 501-513 (2009).
39. Dedmon MM, Christodoulou J, Wilson MR, & Dobson CM. Heat shock protein 70 inhibits alpha-synuclein fibril formation via preferential binding to prefibrillar species. J. Biol. Chem. 280, 14733-14740 (2005).
40. Gao X, et al. Human Hsp70 disaggregase reverses parkinson's-linked α-synuclein amyloid fibrils. Mol. Cell 59, 781-793 (2015).
41. Yagi-Utsumi M, Satoh T, & Kato K. Structural basis of redox-dependent substrate binding of protein disulfide isomerase. Sci Rep 5, 13909 (2015).
42. Wilkinson B & Gilbert HF. Protein disulfide isomerase. Biochim. Biophys. Acta 1699, 35-44 (2004).
43. Robotta M, et al. Alpha-synuclein binds to the inner membrane of mitochondria in an α-helical conformation. Chembiochem 15, 2499-2502 (2014).

44. Bodner CR, Dobson CM, & Bax A. Multiple tight phospholipid-binding modes of alpha-synuclein revealed by solution NMR spectroscopy. J. Mol. Biol. 390, 775-790 (2009).
45. Burmann BM, et al. Regulation of α-synuclein by chaperones in mammalian cells. Nature 577, 127-132 (2020).
46. Ranjan P & Kumar A. The involvement of His50 during protein disulfide isomerase binding is essential for inhibiting α-syn fibril formation. Biochemistry 55, 2677-2680 (2016).
47. Cai J, Yang J, & Jones DP. Mitochondrial control of apoptosis: The role of cytochrome c. Biochim. Biophys. Acta 1366, 139-149 (1998).
48. Gillies LA & Kuwana T. Apoptosis regulation at the mitochondrial outer membrane. J. Cell. Biochem. 115, 632-640 (2014).
49. Khurana R, et al. Mechanism of thioflavin T binding to amyloid fibrils. J. Struct. Biol. 151, 229-238 (2005).
50. Serrano A, et al. Reversal of alpha-synuclein fibrillization by protein disulfide isomerase. Front. Cell Dev. Biol. 8, 726 (2020).
51. Cheng H, Wang L, & Wang CC. Domain a' of protein disulfide isomerase plays key role in inhibiting alpha-synuclein fibril formation. Cell Stress Chaperones 15, 415-421 (2010).
52. Bengoa-Vergniory N, Roberts RF, Wade-Martins R, & Alegre-Abarrategui J. Alpha-synuclein oligomers: A new hope. Acta Neuropathol. 134, 819-838 (2017).
53. Peelaerts W, et al. α-synuclein strains cause distinct synucleinopathies after local and systemic administration. Nature 522, 340-344 (2015).
54. Froula JM, et al. Defining α-synuclein species responsible for Parkinson's disease phenotypes in mice. J. Biol. Chem. 294, 10392-10406 (2019).
55. Zhou W, et al. Methionine oxidation stabilizes non-toxic oligomers of alpha-synuclein through strengthening the auto-inhibitory intra-molecular long-range interactions. Biochim. Biophys. Acta 1802, 322-330 (2010).
56. Carija A, et al. Biasing the native α-synuclein conformational ensemble towards compact states abolishes aggregation and neurotoxicity. Redox Biol 22, 101135 (2019).
57. Ramis R, Ortega-Castro J, Vilanova B, Adrover M, & Frau J. Cu^{2+}, Ca^{2+}, and methionine oxidation expose the hydrophobic α-synuclein NAC domain. Int. J. Biol. Macromol. 169, 251-263 (2021).
58. Yang X, Wang B, Hoop CL, Williams JK, & Baum J. NMR unveils an N-terminal interaction interface on acetylated-α-synuclein monomers for recruitment to fibrils. Proc. Natl. Acad. Sci. U. S. A. 118 (2021).
59. Afitska K, Fucikova A, Shvadchak VV, & Yushchenko DA. Modification of C terminus provides new insights into the mechanism of α-synuclein aggregation. Biophys. J. 113, 2182-2191 (2017).
60. Binolfi A, et al. Interaction of alpha-synuclein with divalent metal ions reveals key differences: A link between structure, binding specificity and fibrillation enhancement. J. Am. Chem. Soc. 128, 9893-9901 (2006).

61. Hoyer W, Cherny D, Subramaniam V, & Jovin TM. Impact of the acidic C-terminal region comprising amino acids 109-140 on alpha-synuclein aggregation in vitro. Biochemistry 43, 16233-16242 (2004).
62. Burre J, Sharma M, & Sudhof TC. Systematic mutagenesis of α-synuclein reveals distinct sequence requirements for physiological and pathological activities. J. Neurosci. 32, 15227-15242 (2012).
63. Zarbiv Y, et al. Lysine residues at the first and second KTKEGV repeats mediate α-synuclein binding to membrane phospholipids. Neurobiol. Dis. 70, 90-98 (2014).
64. Sciacca MF, et al. Lipid-chaperone hypothesis: A common molecular mechanism of membrane disruption by intrinsically disordered proteins. ACS Chem Neurosci 11, 4336-4350 (2020).
65. Nakamura K, et al. Direct membrane association drives mitochondrial fission by the Parkinson disease-associated protein alpha-synuclein. J. Biol. Chem. 286, 20710-20726 (2011).
66. Kamp F, et al. Inhibition of mitochondrial fusion by α-synuclein is rescued by PINK1, Parkin and DJ-1. EMBO J. 29, 3571-3589 (2010).
67. Ryan T, et al. Cardiolipin exposure on the outer mitochondrial membrane modulates α-synuclein. Nat. Commun. 9, 817 (2018).
68. Doherty CPA, et al. A short motif in the N-terminal region of α-synuclein is critical for both aggregation and function. Nat. Struct. Mol. Biol. 27, 249-259 (2020).
69. Kroemer G, Galluzzi L, & Brenner C. Mitochondrial membrane permeabilization in cell death. Physiol. Rev. 87, 99-163 (2007).
70. Vaux DL. Apoptogenic factors released from mitochondria. Biochim. Biophys. Acta 1813, 546-550 (2011).
71. Pfeffer CM & Singh ATK. Apoptosis: A target for anticancer therapy. Int. J. Mol. Sci. 19, (2018).
72. Zhou R, Yazdi AS, Menu P, & Tschopp J. A role for mitochondria in NLRP3 inflammasome activation. Nature 469, 221-225 (2011).
73. Gong Z, Pan J, Shen Q, Li M, & Peng Y. Mitochondrial dysfunction induces NLRP3 inflammasome activation during cerebral ischemia/reperfusion injury. J. Neuroinflammation 15 (2018).
74. Yu JW & Lee MS. Mitochondria and the NLRP3 inflammasome: Physiological and pathological relevance. Arch. Pharm. Res. 39, 1503-1518 (2016).
75. Wang W, et al. Caspase-1 causes truncation and aggregation of the Parkinson's disease-associated protein α-synuclein. Proc. Natl. Acad. Sci. U. S. A. 113, 9587-9592 (2016).
76. Grunewald A, Kumar KR, & Sue CM. New insights into the complex role of mitochondria in Parkinson's disease. Prog. Neurobiol. 177, 73-93 (2019).
77. Park JS, Davis RL, & Sue CM. Mitochondrial dysfunction in Parkinson's disease: New mechanistic insights and therapeutic perspectives. Curr. Neurol. Neurosci. Rep. 18, 21 (2018).
78. Diepenbroek M, et al. Overexpression of the calpain-specific inhibitor calpastatin reduces human alpha-synuclein processing, aggregation and synaptic impairment in [A30P]αsyn transgenic mice. Hum. Mol. Genet. 23, 3975-3989 (2014).

79. Zhang Z, et al. Ca^{2+} modulating α-synuclein membrane transient interactions revealed by solution NMR spectroscopy. Biochim. Biophys. Acta 1838, 853-858 (2014).
80. Zhang Z, et al. Calcium accelerates snare-mediated lipid mixing through modulating α-synuclein membrane interaction. Biochim. Biophys. Acta, Biomembr. 1860, 1848-1853 (2018).
81. Bai J, Zhang Z, Liu M, & Li C. α-synuclein-lanthanide metal ions interaction: Binding sites, conformation and fibrillation. BMC Biophys. 9, 1 (2015).
82. Arai M, Ferreon JC, & Wright PE. Quantitative analysis of multisite protein-ligand interactions by NMR: Binding of intrinsically disordered p53 transactivation subdomains with the TAZ2 domain of CBP. J. Am. Chem. Soc. 134, 3792-3803 (2012).
83. Iwahara J, Tang C, & Marius Clore G. Practical aspects of ^{1}H transverse paramagnetic relaxation enhancement measurements on macromolecules. J. Magn. Reson. 184, 185-195 (2007).
84. Ghio S, et al. Cardiolipin promotes pore-forming activity of alpha-synuclein oligomers in mitochondrial membranes. ACS Chem. Neurosci. 10, 3815-3829 (2019).

Table

Table 1. Aggregation kinetics

Protein	t_{lag}[1] (hr)	k[2]	$t_{1/2}$ (hr)
FL-α-syn	7.4±0.4	0.65±0.03	10.5±0.3
CT-α-syn	2.1±0.3	1.1±0.1	4.0±0.3
Y39E-α-syn	ND[4]	ND[4]	ND[4]
FL-α-syn +PDI	23±2	0.28±0.05	30±3
CT-α-syn +PDI	4.0±0.3	0.7±0.1	6.9±0.6
Y39E-α-syn+PDI	36±2	0.21±0.03	46±1

[1] Lag time.

[2] Elongation rate constant.

[3] Half time of aggregation.

[4] Plateau was not reached.

Figures

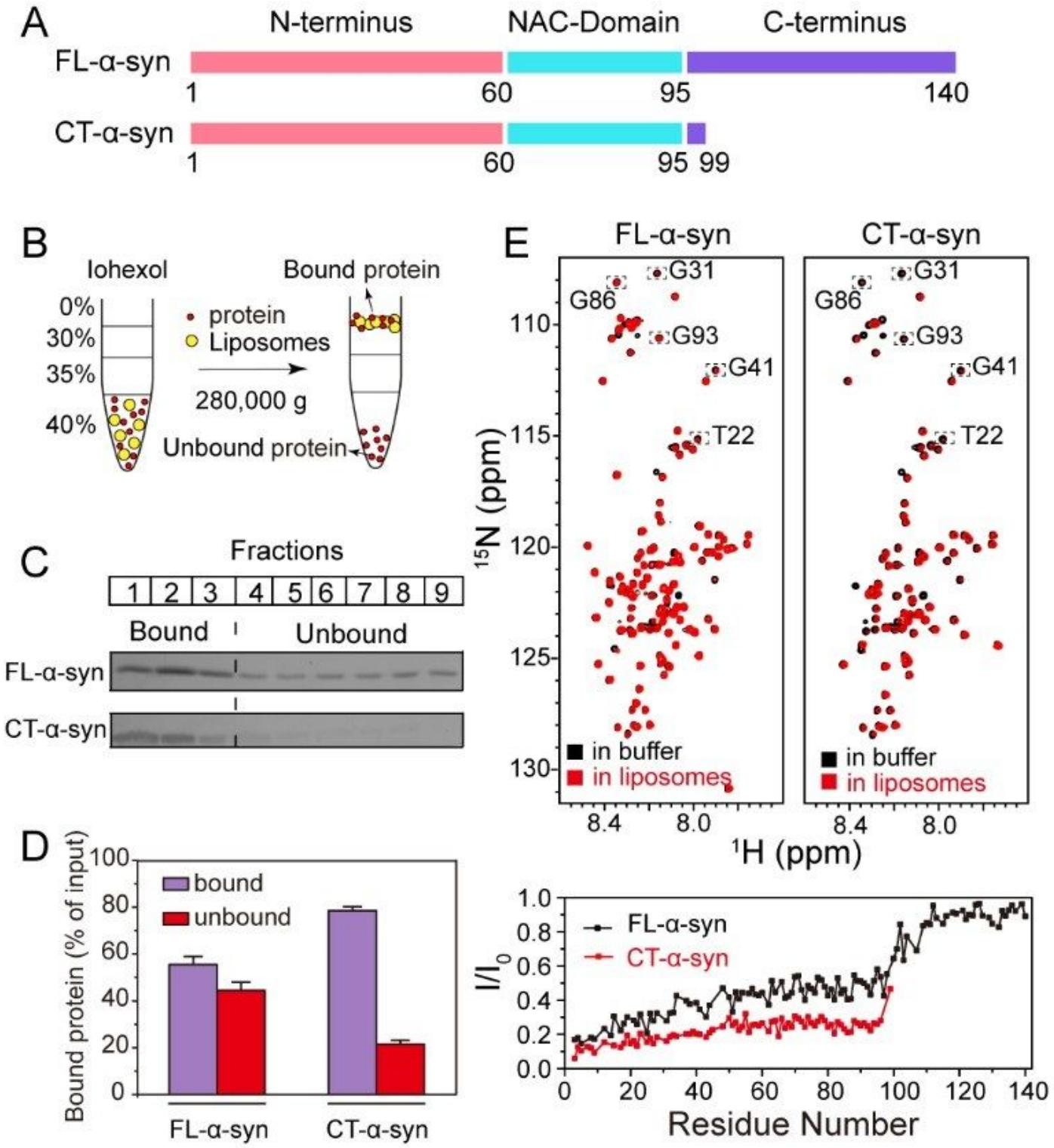

Figure 1

Stronger CT-α-syn membrane interaction.

(A) Primary structure schematic of FL- (top) and CT-α-syn (bottom). (B) Cartoon of coflotation assay. (C) SDS-PAGE of fractions post centrifugation. (D) Lipid-bound (black) and unbound protein (red) from SDS-PAGE data. Uncertainties are the standard error of the mean from three independent trials. (E) Overlaid ^{1}H-

^{15}N HSQC spectra of 0.12 mM ^{15}N-enriched FL- (left) and CT-α-syn (right) in the absence (black) and presence (red) of 12 mM POPC/CL (9:1 molar ratio) liposomes and residue-resolved attenuation (I/I_0) of FL- (black) and CT-α-syn (red) upon adding liposomes. Values <1.0 indicate interactions. Representative cross-peak broadening/disappearance are shown in dotted boxes.

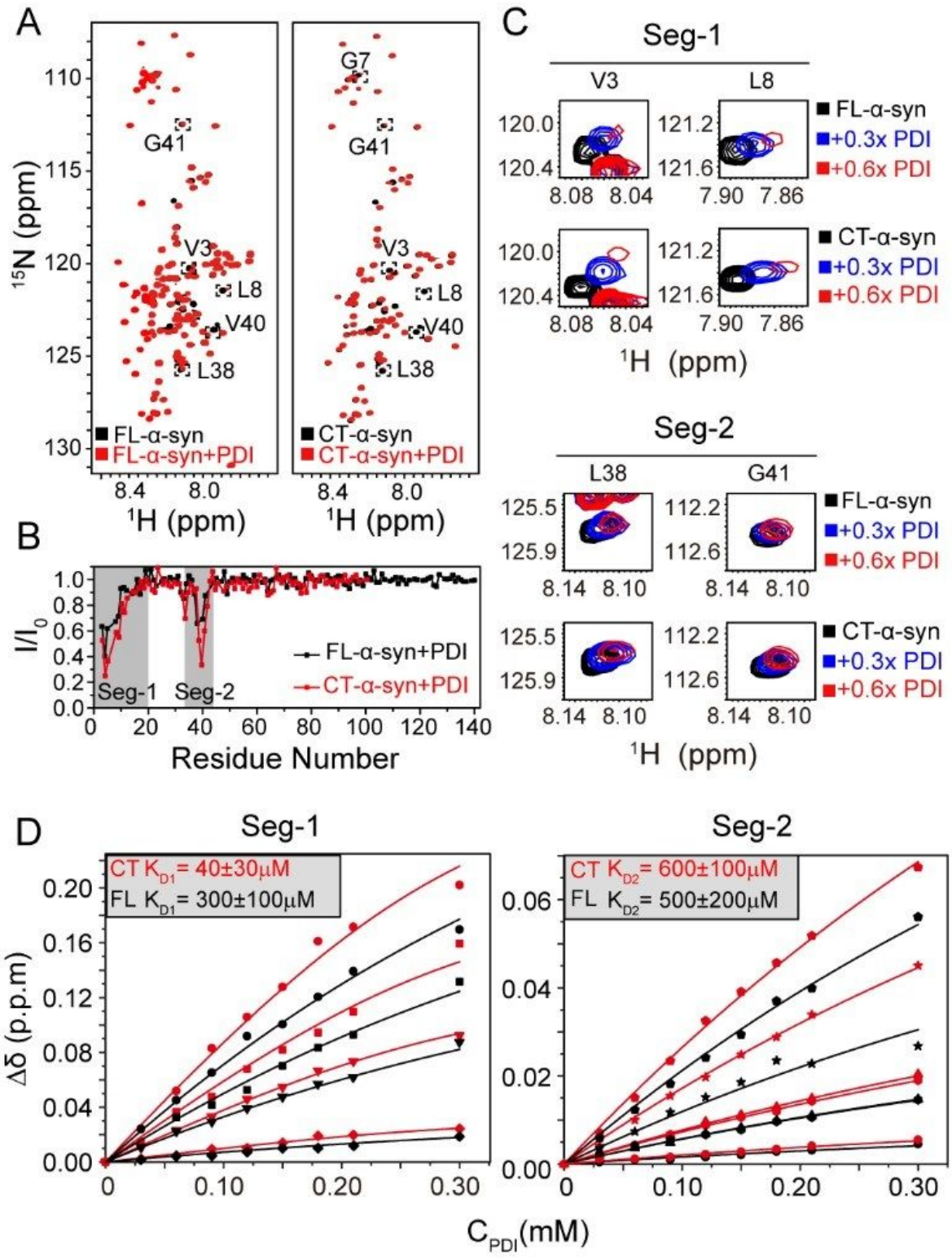

Figure 2

Stronger interaction of CT-α-syn with PDI.

(A) Overlay of ^{1}H-^{15}N HSQC spectra of 0.30 mM ^{15}N-enriched FL- (left) and CT-α-syn (right) in the absence (black) and presence (red) of 0.15 mM PDI. Perturbed residues are surrounded by a dotted box. (B) Residue-resolved signal attenuation (I/I_0) of FL- (black) and CT-α-syn (red) upon adding 0.15 mM PDI. Values <1.0 indicate interactions. Binding regions are colored gray. (C) Representative ^{1}H-^{15}N HSQC cross-peaks within segments 1 and 2 of FL- (top) and CT-α-syn (bottom) at two PDI ratios. (D) Chemical shift perturbations of residues within segment 1 (V3, M5, L8 and S9) and 2 (V37, L38, V40, G41 and T44) of FL- and CT-α-syn as a function of PDI concentration. K_D values are from curve fitting.

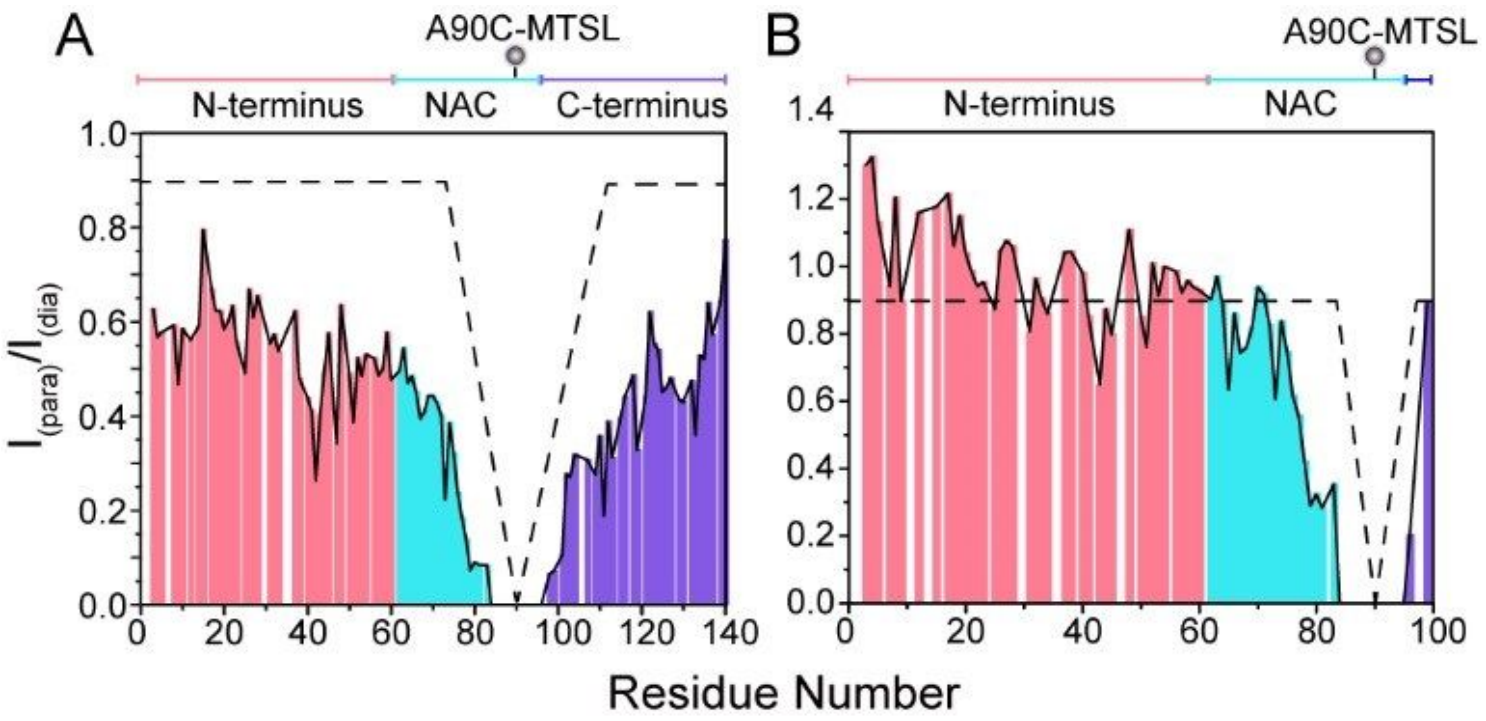

Figure 3

A more extended conformation for CT-α-syn.

(A-B) Intramolecular PRE intensity ratios of backbone amides in FL- (A) and CT-α-syn variants (B) possessing a MTSL spin label at A90C. Pink, blue, and burgundy identify the N-terminal, NAC and the C-terminal domain, respectively. Schematic diagram of sequence domain is shown above each plot. Circles indicate locations of the label.

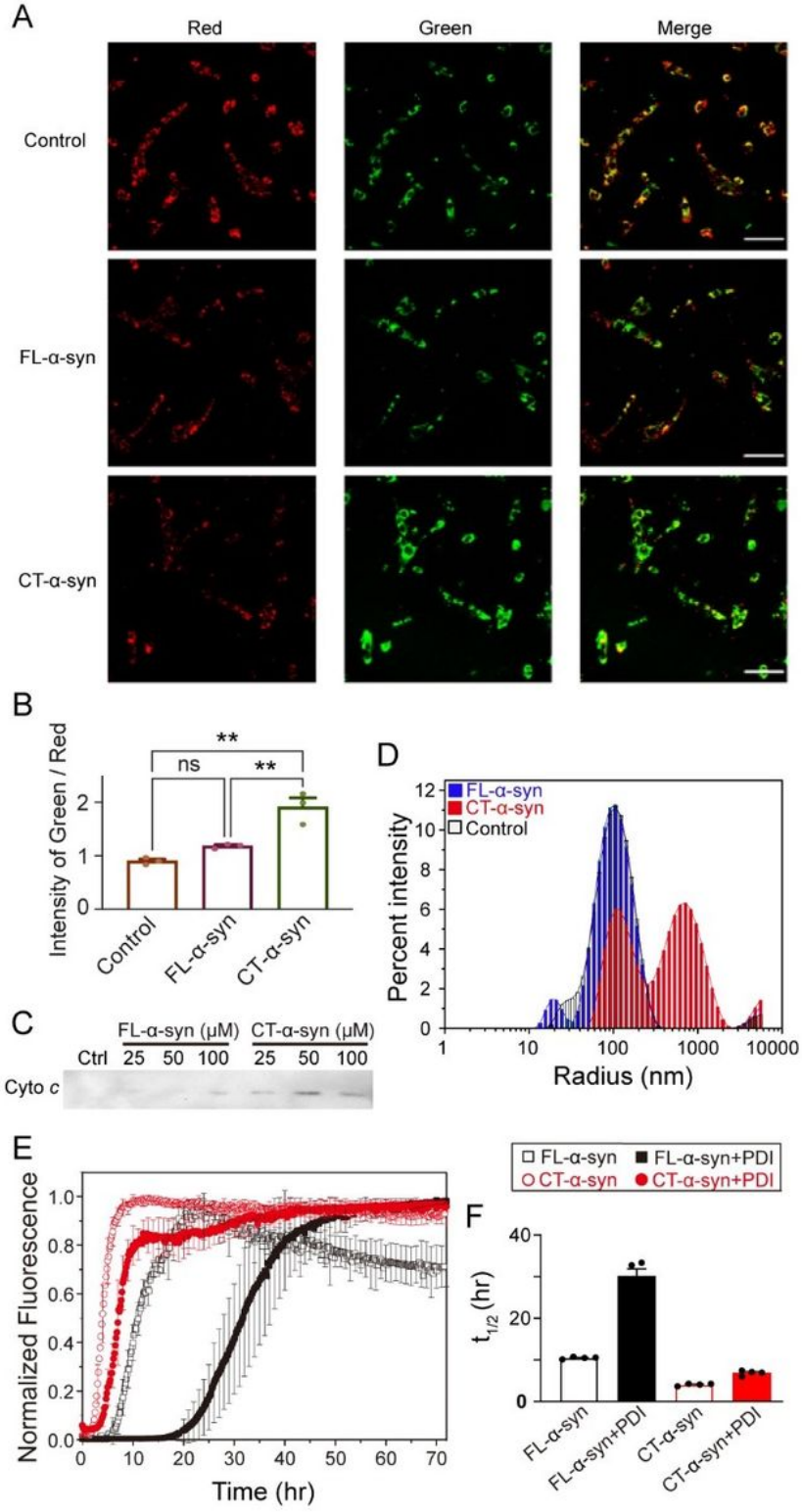

Figure 4

Physiological and pathological consequences of CT-α-syn.

(A) Representative confocal images of JC-1-stained SK-N-SH cells after 5 h treatment with 50 μM FL- α-syn and CT-α-syn at 37 °C. (B) Integrated fluorescence intensities of five random visual fields were analyzed with Image J software using the mean ratio of green to red fluorescence to indicate

mitochondrial damage. Scale bar = 2 μm. Uncertainties are the standard error of the mean from three independent experiments. (*p < 0.05; **p < 0.01; ns, not significant). (C) Cytochrome *c* levels were assessed by WB after incubating isolated mitochondria with increasing concentrations of FL- and CT-α-syn at 37 °C for 1 h. Unincubated mitochondria served as positive controls. (D) DLS particle size of POPC/CL (9:1 mole ratio) liposomes alone (blank), or after incubation with FL- (blue) or CT-α-syn (red) for 30 min measured. (E) Aggregation kinetics of FL- and CT-α-syn in the absence (open) and presence (filled) of equimolar mixtures with PDI monitored by ThT fluorescence. (F) Half-time ($t_{1/2}$) of aggregation. Uncertainties are the standard error of the mean from four independent experiments.

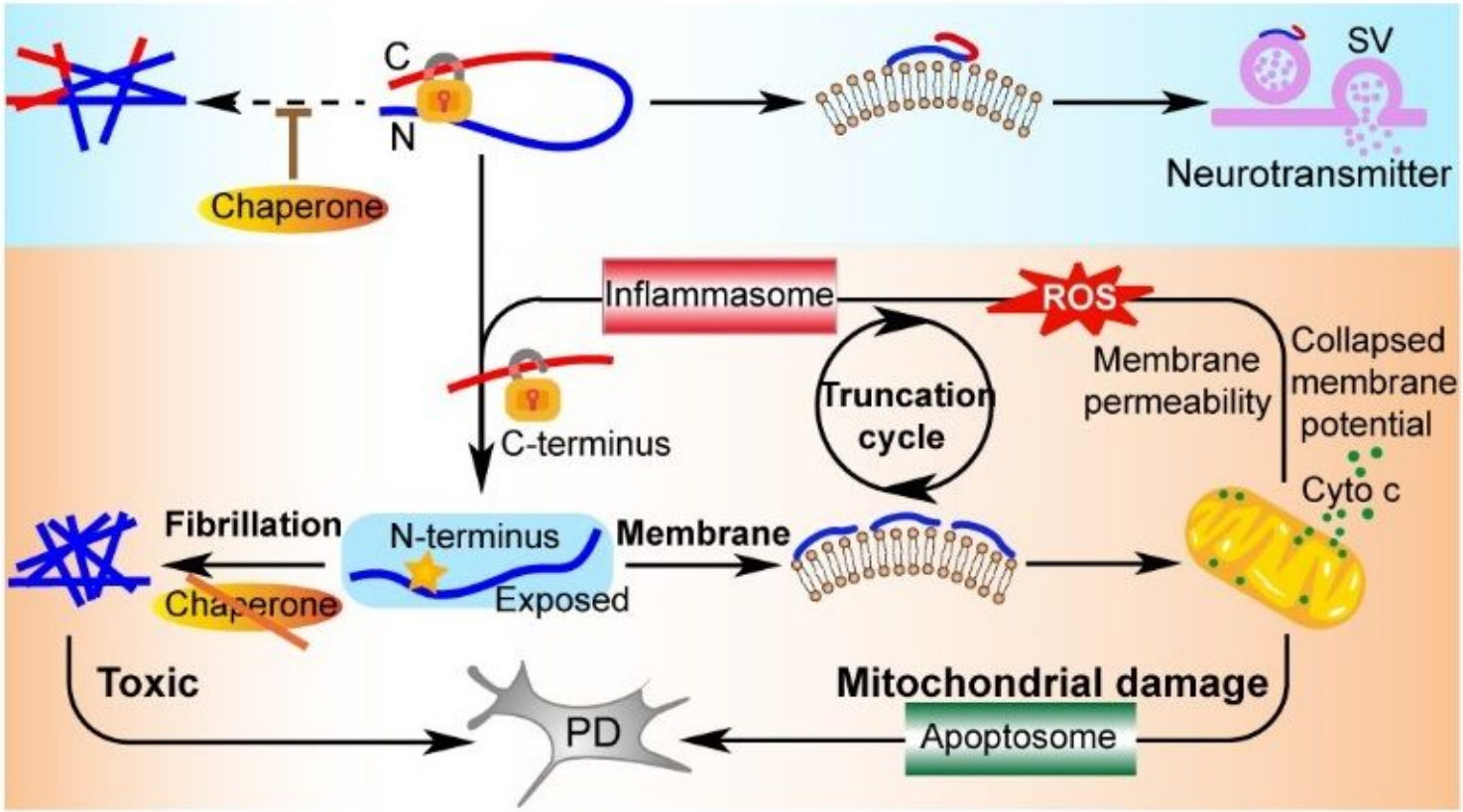

Figure 5

Mechanism of CT-α-syn involvement in the pathogenesis of PD.

Interaction between FL-α-syn and membranes is critical for neurotransmitter release, and fibrillation of FL-α-syn is inhibited by chaperones. When the C-terminus is truncated, the interaction with membranes and chaperones becomes stronger, leading to diminished inhibition of fibrillation and mitochondrial damage. The inflammasome is then activated causing truncation of more α-syn, forms a vicious cycle that contributes to pathogenesis.

Supplementary Files

This is a list of supplementary files associated with this preprint. Click to download.

- TableOfContent.jpg
- CtruncationSI20220112.docx